Available online at www.sciencedirect.com
ScienceDirect
Trans. Nonferrous Met. Soc. China 28(2018) 1265−1274
Transactions of Nonferrous Metals Society of China
www.tnmsc.cn

# Thermal decomposition kinetics of basic carbonate cobalt nanosheets obtained from spent Li-ion batteries: Deconvolution of overlapping complex reactions

Hossein EBRAHIMZADE[1], Gholam Reza KHAYATI[2], Mahin SCHAFFIE[3]

1. Department of Mineral Industries Research Center,
Shahid Bahonar University of Kerman, P. O. Box No. 76135-133, Kerman, Iran;
2. Department of Materials Science and Engineering,
Shahid Bahonar University of Kerman, P. O. Box No. 76135-133, Kerman, Iran;
3. Department of Chemical Engineering,
Shahid Bahonar University of Kerman, P. O. Box No. 76135-133, Kerman, Iran

Received 24 March 2017; accepted 18 July 2017

**Abstract:** A new non-isothermal method of kinetic analysis was employed to investigate the thermal decomposition kinetic modeling of the basic carbonate cobalt nanosheets (n-BCoC) synthesized from spent lithium-ion batteries (LIBs). Fraser–Suzuki function was applied to deconvoluting overlapping complex processes from the overall differential thermal curves obtained under the linear heating rate conditions, followed by the kinetic analysis of the discrete processes using a new kinetic analysis method. Results showed that the decomposition of n-BCoC in air occurred through two consecutive reactions in the 136−270 °C temperature intervals. Decomposition started by hydroxide component ($Co(OH)_2$) decomposition until to 65% and simultaneously carbonate phase decarbonation began. The process was continued by $CO_2$ evolution and finally carbonate cobalt nanosheets have been produced. The reaction mechanism of the whole process can be kinetically characterized by two successive reactions: a phase boundary contracting reaction followed by an Avrami−Erofeev equation. Mechanistic information obtained by the kinetic study was in good agreement with FT-IR (Fourier transform infrared spectroscopy) and SEM (scanning electron microscopy) results.
**Key words:** kinetic modeling; basic carbonate cobalt nanosheets (n-BCoC); overlapping reactions; spent lithium-ion battery

## 1 Introduction

Recently, much more attention has been paid to the recovery of precious metals, especially cobalt from spent lithium-ion batteries, in the form of metal oxides nanoparticles [1,2]. Cobalt is one of the main metal constituents of LIBs cathode material and therefore, the recovery of cobalt oxide precursors and investigation of their decomposition reaction mechanism have great importance from the economic viewpoint as well as environmental aspects. Cobalt oxide has been widely used in heterogeneous catalysis, electrochromic devices, gas sensors and electrochemistry [3,4]. Among the various cobalt oxide precursors, hydroxide carbonate is the most desirable, due to facile synthesis and no toxic product gasses, e.g., nitrogen oxide and sulfur dioxide. Preparation of hydroxide carbonates by emphasis on their crystallography, structural information, chemical reactivity, surface and electrochemical properties has been extensively investigated [5−8], but their thermal decomposition kinetics with more details has been less considered. The thermal decomposition of BCoC, i.e., $Co(OH)_x(CO_3)_{0.5(2-x)}\cdot nH_2O$ is the main step of spinel cobalt oxide ($Co_3O_4$) preparation from hydroxide carbonate precursors. Detailed kinetic analysis of BCoC decomposition can present valuable information in order to synthesize the cobalt oxide nanoparticles with the aim of morphology control, catalytic, magnetic, electrochemical properties and energy conservation aspects.

To the best of our knowledge, a few studies have investigated the kinetic analysis of BCoC using mean activation energy or model fitting method. It was reported that the thermal decomposition of BCoC is a complex reaction and includes two consecutive steps, i.e., dehydroxylation and decarbonation occur in the temperature range of 225−375 °C under the flowing of

**Corresponding author:** Gholam Reza KHAYATI; Tel: +98-915-1903477; Fax: +98-341-2114053; E-mail: khayatireza@gmail.com, khayati@uk.ac.ir
DOI: 10.1016/S1003-6326(18)64733-8

$O_2$ gas [9]. Using magnetic susceptibility measurement analysis, MEHANDJIEV and NIKOLOVA-ZHECHEVA [10], concluded that the basic cobalt carbonate decomposition mechanism in vacuum was similar to that in air, i.e., the process begins with the formation of $Co^{3+}$ ions in the octahedral coordination. ROMERO et al [11] proposed that the BCoC thermal decomposition reaction includes dehydroxylation and decarbonation steps which obey $D_5$ mechanism with activation energies of (144±1) and (174±1) kJ/mol, respectively.

It is necessary to note that the kinetic analysis of complex reactions by means of ordinary methods, using mean activation energy for the whole of reaction progress, results in unsound reaction kinetic model(s). Accordingly, in order to correct kinetic modeling, deconvolution of complex overlapping reactions must be performed kinetically (e.g., changing in the experimental condition) or by the mathematical method. PEREJON et al [12] showed that the conventional functions such as Lorentzian and Gaussian ones, fit the overlapped kinetic curves inaccurately and subsequent kinetic analysis yields incorrect parameters. While the Fraser−Suzuki function can properly deconvolute the overlapping reactions without changing their kinetic model.

In this study, as an innovative method, n-BCoC, i.e., $Co(OH)_{1.02}(CO_3)_{0.49}\cdot 0.29H_2O$ precursor, was prepared by selective precipitation of spent Li-ion batteries leaching solution. Finally, overlapping thermal decomposition of n-BCoC was deconvoluted by Fraser−Suzuki function and an advanced kinetic modeling method was used to study the individual reaction kinetics, separately.

## 2 Experimental

### 2.1 Material and experimental procedure

To synthesize n-BCoC, mixed-waste mobile phone batteries (LIBs) were first discharged and dismantled manually to separate into cathodes, anodes, plastic separators and metal cases [13−15]. Then, the cathodic material was collected and treated with *N*-methyl-2-pyrrolidone (NMP, Merck, 99.5%) at 60 °C for 1 h. After filtration, the resulted powder was dried at 50 °C for 24 h and sieved with the screen of 0.5 mm. Thermal pretreatment of resulting powder was carried out at 700 °C for 5 h in a muffle to eliminate carbon, polyvinylidene fluoride (PVDF) and solvent residue. The resultant cathodic active powder was leached with 2 mol/L NaOH solution to selectively dissolve the remaining aluminum pieces. Then, the filter residue was leached with 2 mol/L $H_2SO_4$ (Merck, 95%−97.0%) and 4% $H_2O_2$ (volume fraction) (Sigma-Aldrich, 30%) at 70 °C for 2 h. The pH of leach liquor was adjusted to 5 with 2 mol/L NaOH solution in order to make the impurity ions form $Al(OH)_3$, MnOOH, and $Ni(OH)_2$ precipitates. Cobalt content solution was purified from impurities and diluted with distilled water to obtain a solution with $3894\times10^{-6}$ cobalt ion. The absence of $Co^{3+}$ was confirmed by a standard solution of ferrous ammonium sulfate and potentiometric back titrating the excess $Fe^{2+}$ with a standard solution of $K_2Cr_2O_7$. Finally, n-BCoC precursor prepared by adding a mixture of 45 mL 0.1 mol/L NaOH (Merck, >99.0%) aqueous solution and 0.24 g $Na_2CO_3$ (Merck, >99.0%) dropwise with the adding rate of 0.3 g/(L·min) into 70 mL of last solution under the pure $N_2$ gas flowing (30 mL/min) and ultrasonic irradiation (AT-LQ100, 25 kHz, 360 W). The as-formed precipitate (pink) was aged in the mother liquor for 1 h. During both addition and aging periods, the mixture was stirred under the ultrasonic waves and reaction solution purged with purified $N_2$. Finally, the precipitate was centrifuged and washed three times with deionized water to remove different soluble salts and excess of $CO_3^{2-}$ ions and then dried at 50 °C to a constant mass. $Co_3O_4$ nanosheets were papered by heat treatment of dry precipitate at 300 °C for 2 h in air.

### 2.2 Characterization

The quantitative content of metals in the powder of spent LIBs (Table 1) and cobalt ion concentration in the leaching solution were assessed by atomic absorption spectrometry (AA 240-Varian). The mass fraction of carbon in the prepared samples was measured in a CHN analyzer (Elementar, Vario EL III). To study the kinetic of n-BCoC decomposition, (7±0.5) mg of the sample was analyzed through DSC−TGA (Differential Scanning Calorimetry–Thermal Gravimetry Analysis, NETZSCH STA409PG) at four heating rates of 5, 10, 15 and 20 °C/min under the air flowing rate of 50 $cm^3$/min from 25 to 450 °C. The crystalline structure, morphology and crystalline size of BCoC precursor and $Co_3O_4$ nanosheets, were characterized by XRD using Philips X'Pert-MPD system diffractometer (Cu $K_\alpha$, $\lambda$=1.5418 Å) and HRSEM (Hitachi-S4160). FT-IR spectra were recorded on a Bruker Tensor 27 spectrometer with DLATGS detector, using a KBr pellet technique over the frequency range of 400−4000 $cm^{-1}$. FT-IR spectra of samples isothermally heated at 25, 150 and 300 °C for 2 h, were measured to confirm the mechanism of phase evolution.

**Table 1** Chemical analysis of main metals in waste LIBs cathodic powder (mass fraction, %)

| Co | Li | Ni | Mn | Al |
|---|---|---|---|---|
| 35.66 | 5.92 | 10.84 | 11.26 | 0.68 |

## 3 Theoretical

### 3.1 Peak deconvolution

Deconvolution of kinetically independent overlapping processes was carried out by Fraser−Suzuki fitting function as follows [16]:

$$y = a_0 \exp\left\{-\ln 2\left[\left(\ln\left(1+a_3\frac{x-a_1}{0.5a_2}\right)\right)\Big/a_3\right]^2\right\} \quad (1)$$

where $a_0$, $a_1$, $a_2$ and $a_3$ are amplitude, position, half-width and asymmetry of the curve, respectively. Origin Lab pro8.1 software was used for nonlinear least square curve fitting.

### 3.2 Kinetic analysis

The rate ($v$) of a thermally stimulated, single particle, single step solid-state reaction can be described by the following basic kinetic equation:

$$v = \frac{\mathrm{d}\alpha}{\mathrm{d}t} = k(T)f(\alpha) \quad (2)$$

where $\alpha$ is the fraction of reaction, $t$ is the reaction time, $T$ is the temperature, $f(\alpha)$ is the kinetic model and $k(T)$ is the rate coefficient of reaction. Rate coefficient of solid-state reactions is typically expressed by the Arrhenius equation:

$$k(T) = A\exp\left(-\frac{E_\mathrm{a}}{RT}\right) \quad (3)$$

where $A$ is the pre-exponential (frequency) factor, $R$ is the mole gas constant (8.314 J/(mol·K)) and $E_\mathrm{a}$ is the apparent activation energy.

Reaction rate equation in linear heating rate condition ($\beta$=d$T$/d$t$=cons.) at given fraction of reaction $\alpha$, is as follows:

$$\frac{\mathrm{d}\alpha}{\mathrm{d}t} = \beta\frac{\mathrm{d}\alpha}{\mathrm{d}T} = k(T)f(\alpha) \quad (4)$$

The advanced Vyazovkin [17] method, which assumes $E_\mathrm{a}$ to be constant only for a small segment of $\Delta\alpha$ and uses integration over the small time segments, was used for evaluation of activation energy changes with $\alpha$:

$$\int_{\alpha-\Delta\alpha}^{\alpha}\frac{\mathrm{d}\alpha}{f(\alpha)} = A_\alpha\int_{t_{\alpha-\Delta\alpha}}^{t_\alpha}\exp\left(-\frac{E_\mathrm{a}}{RT_{i(t)}}\right)\mathrm{d}t = A_\alpha J[E_\mathrm{a},\ T_{i(t_\alpha)}] \quad (5)$$

where $J[E_\mathrm{a},\ T_{i(t_\alpha)}]$ is the temperature integral for $\alpha$ and the heating rate of $\beta_i$. $E_\mathrm{a}$ can be determined by minimizing the following function:

$$\Phi(E_\mathrm{a},\ T_\alpha) = \left|\sum_{i=1}^{n}\sum_{j\neq i}^{m}\frac{J\left[E_\mathrm{a},\ T_{i(t_\alpha)}\right]}{J\left[E_\mathrm{a},\ T_{j(t_\alpha)}\right]}\right| \quad (6)$$

By consideration of variable activation energy concept and temperature dependency of pre-exponential factor in solid-state reactions, ARSHAD and MAAROUFI [18] introduced new kinetic modeling method as

$$h(\alpha) = \frac{f'(\alpha)}{f(\alpha)} = \frac{1}{(\mathrm{d}\alpha/\mathrm{d}t)_\alpha}\cdot\left[\frac{\beta\mathrm{d}E_\mathrm{a}/\mathrm{d}T}{RT_\alpha} - \frac{\beta E_\mathrm{a}}{RT_\alpha^2} + \frac{(\mathrm{d}^2\alpha/\mathrm{d}t^2)_\alpha}{(\mathrm{d}\alpha/\mathrm{d}t)_\alpha}\right] \quad (7)$$

Equation (7) was entirely obtained by the isoconversional parameters and accurately modeled the kinetics of complex solid-state reactions [19]. Moreover, it can be used for isothermal, non-isothermal, multi-step and as well as single step reactions. By definition, $h(\alpha)$ and the subsequently numerical integration, $f(\alpha)$, are described as follows:

$$h(\alpha) = \frac{f'(\alpha)}{f(\alpha)},\ f(\alpha) = \exp(\int_0^1 h(\alpha)\mathrm{d}\alpha) \quad (8)$$

## 4 Results and discussion

### 4.1 Characterization of precursor and product

Figure 1 shows the FT-IR spectra obtained for n-BCoC and its calcination products at 150 and 300 °C for 2 h. The spectrum (Fig. 1(a)) shows the $CoCO_3$, water and hydrogen-bonded OH groups vibrational frequencies [5]. The intense and relatively broad band around 1470 cm$^{-1}$ is assigned to stretching vibration mode of the polar $CO_3^{2-}$ group. Splitting of this band (Fig. 1(b)) indicates a decrease in the symmetry of the carbonate groups as a result of temperature increasing and reaction progress. Shoulders at around 2847 and 2928 cm$^{-1}$ from hydrogen bonding in the interlayer indicate the presence of intercalated water molecules in the precursor. As the temperature rises the intensities of these bands relatively increase due to the hydrogen bond cleavage (Fig. 1(b)). The sharp band at 829.94 cm$^{-1}$ is attributed to $v_2$ bending mode of ($CO_3^{2-}$) units, and the minor bands at around 1073 and 686 cm$^{-1}$ can be assigned to $v$(C═O) and $\rho$(OCO), respectively, while the bands at 936 and 517 cm$^{-1}$ are ascribed to $\delta$(M—OH) and $\rho_\mathrm{w}$(M—OH) bending modes [20]. On the other hand, absorptions of $Cl^-$, $NO_3^-$ and $SO_4^{2-}$ species are not detected.

The FT-IR spectrum at 150 °C (Fig. 1(b)) displays the decrease in O—H and OCO stretching vibration absorption band intensity of precursor at 3555.78 and

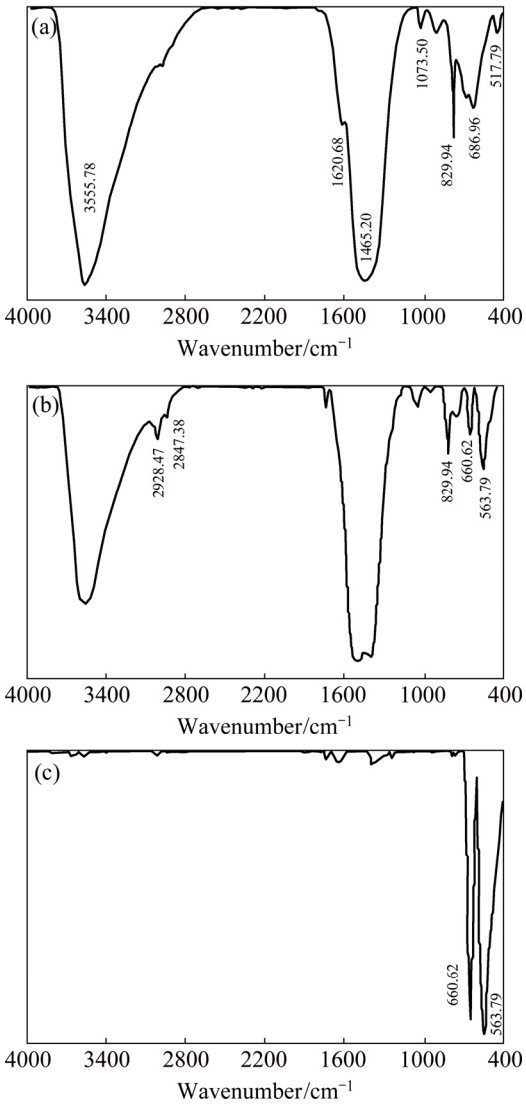


**Fig. 1** FT-IR spectra of precursor (a), and products after calcination of precursor at 150 °C (b) and 300 °C (c) for 2 h in air

1465.2 $cm^{-1}$, respectively. Moreover, the intensity of the characteristic vibrational band of structural O—H, i.e., the peak at around 1620 $cm^{-1}$ (bending mode of water molecules), decreases with increasing temperature. Therefore, it can be concluded that the dehydration of water molecules was completed and decomposition of the anhydrous precursor was started before 150 °C which is consistent with DSC−TG thermoanalysis curves (Fig. 2). The FT-IR spectrum at 300 °C (Fig. 1(c)) reveals the absence of structural O—H group vibration frequency and absorption bands of carbonate group. The spectrum clearly displays the vibrational mode frequencies of $Co_3O_4$ at 563 and 660 $cm^{-1}$.

XRD patterns of precursor and its calcination product are shown in Fig. 3. Diffractogram (Fig. 3(a)) with broad and relatively low-intensity reflections with some degree of crystallinity indicates the interlayer water incorporated in the n-BCoC structure. All the diffraction peaks of which are consistent with the BCoC (JCPDS card No. 48−0083). The mean crystalline size of precursor platelets was calculated to be about 10 nm using the Debye−Scherer equation [21].

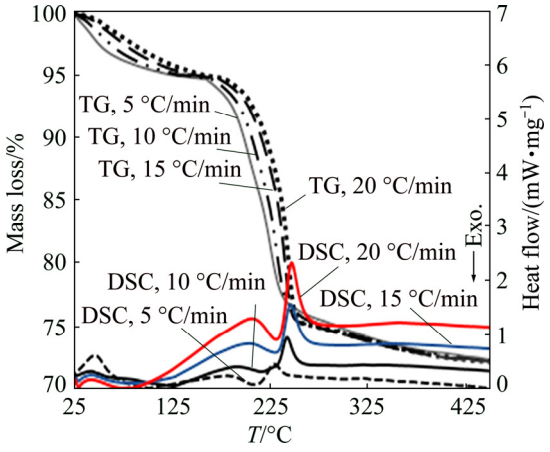


**Fig. 2** Typical thermal analysis curves, DSC−TG of precursor under air flowing of 50 $cm^3$/min at different heating rates

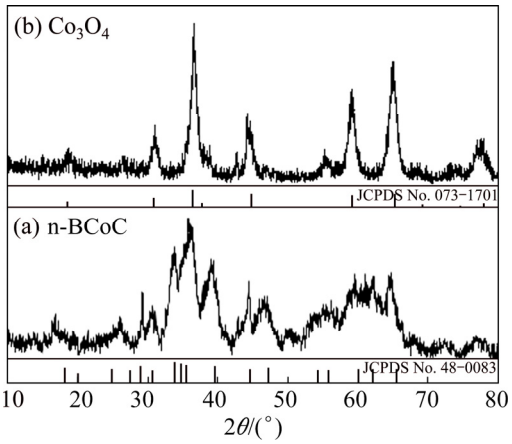


**Fig. 3** XRD pattern of precursor (a) and product after calcination at 300 °C for 2 h in air (b)

The XRD pattern of n-BCoC at 300 °C (Fig. 3(b)) reveals the complete development of a new phase, with diffraction patterns that exhibit characterized lines, matches well with the $Co_3O_4$ (JCPDS card No. 073−1701). The results of TG, XRD and FT-IR with CHN analysis (absence of nitrogen, *w*(carbon)= 5.28%) revealed the precursor to be $Co(OH)_{1.02}(CO_3)_{0.49}\cdot 0.29H_2O$. Accordingly, 22.87% of mass loss observed in TGA curves in temperature interval of 136−270 °C was related to the following balanced chemical equation which includes two consecutive sub-reactions (Fig. 2(DSC curves)):

$$Co(OH)_{1.02}(CO_3)_{0.49}(s)+1/6O_2(g)\rightarrow 1/3Co_3O_4(s)+0.51H_2O(g)+0.49CO_2(g) \quad (9)$$

TG and DSC curves of n-BCoC at heating rates of

5, 10, 15 and 20 °C/min in the air are shown in Fig. 2. The curves indicate that n-BCoC decomposes via three endodermic mass-loss processes over the temperature range from 25 to 270 °C which include dehydration and two overlapping endothermic decomposition processes (Fig. 2), showing peaks at 201 and 222 °C ($\beta$=5 °C/min) respectively. Since there is not any thermal effect in DSC, a little mass change beyond 270 °C can be attributed to the gas evolution, e.g., $CO_2$ formation due to decomposition of some residual carbonate groups or $O_2$ from the non-stoichiometric product ($Co_3O_{4+x}$) [22]). The precursor does not experience another mass change process beyond 450 °C. The thermal effect in the range of 25−110 °C (Fig. 2) is an endothermic process with about 5% mass-loss of precursor and can be related to the dehydration process of intercalated water. In fact, the DTG (differential thermal gravimetry) derivatogram (Fig. 4) at $\beta$=5 °C/min shows that the thermal decomposition of the precursor is a complex overlapped reaction.

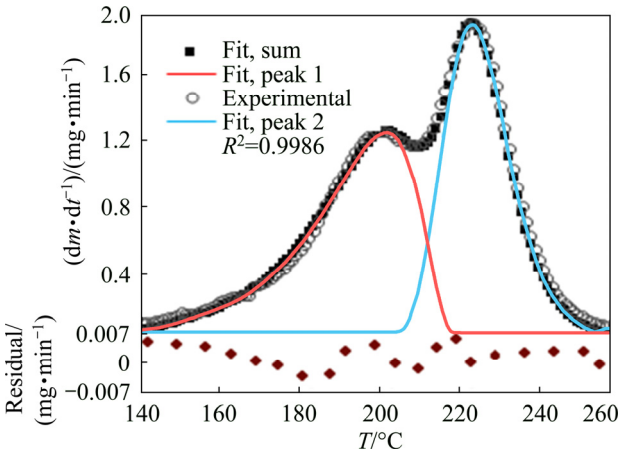


**Fig. 4** Typical DTG curve of precursor (circle) at heating rate of 5 °C/min and corresponding Fraser–Suzuki functions (red and blue lines) and their sum (black square) used for fitting experimental curve (Residuals are plotted underneath of the curve)

### 4.2 Deconvolution of overlapping thermal decomposition process and kinetic modeling

Overlapping consecutive reactions in DTG curve deconvoluted with Fraser–Suzuki function are shown in Fig. 4. As can be seen, the curves have been accurately fitted with residuals better than ±0.007. After deconvolution fitting of other heating rate peaks, each individual step was independently analyzed with isoconversional methods. Figure 5 shows the typical $\alpha$−$T$ curves of dehydration, first and second decomposition reaction steps that evaluated from the TGA and deconvoluted peaks at 5 °C/min. These data were used for the calculation of $E$ vs $\alpha$ curves by the advanced Vyazovkin method.

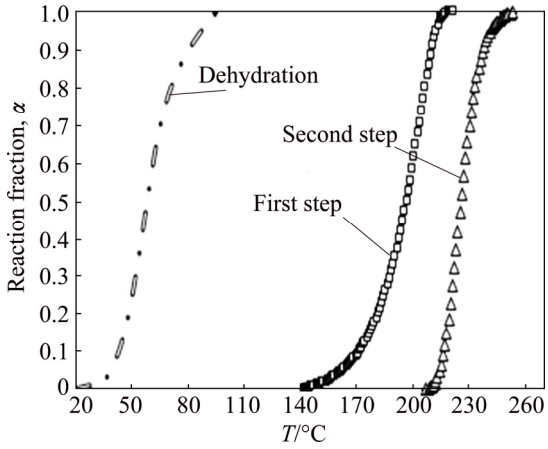


**Fig. 5** $\alpha$−$T$ curves of dehydration, first and second steps of deconvoluted peaks at 5 °C/min

The changes of $E_a$ as a function of reaction fraction, $\alpha$, are plotted in Fig. 6. The average activation energies of the dehydration, first and second steps of precursor decomposition were calculated to be (83±1), (105±1) and (160±1) kJ/mol, respectively. These values are comparable to the reported values of BCoC decomposition [11,23].

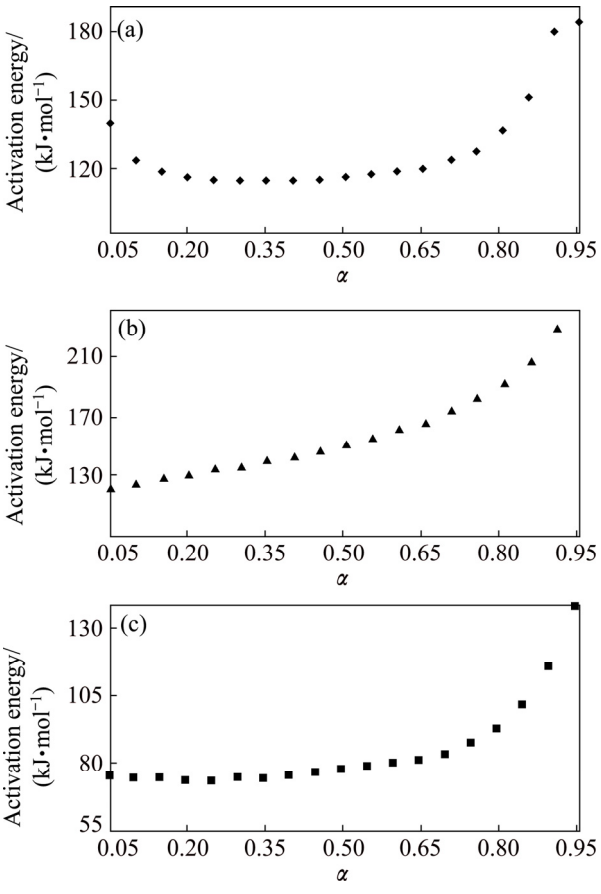


**Fig. 6** Activation energy of dehydration (a), first (b) and second (c) steps of n-BCoC decomposition as function of reacted fraction calculated by AIC isoconversional method

Dehydration reaction proceeds approximately with a constant activation energy (Fig. 6(c)). As shown from Fig. 6(a), the activation energy of the first decomposition process (dehydroxylation) relatively remains constant through $0.05<\alpha<0.85$. According to the schematic representation of basic cobalt carbonate structure shown in Fig. 7, the precursor has a layered, planar structure and the distance between planes is 4.6−6.9 Å with different ion compositions [24]. Consequently, the water molecules (intercalated water molecules diameter of 2.75 Å) can transport easily to the atmosphere of reaction through sheet interlayer channels.

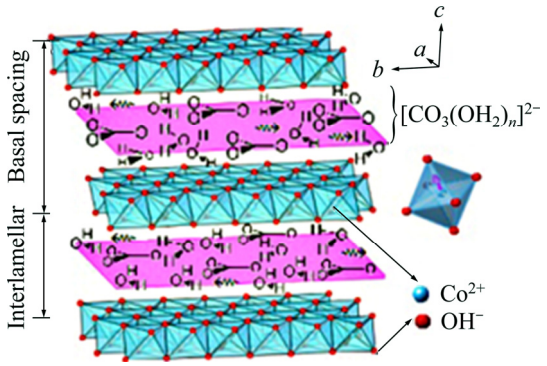


**Fig. 7** Schematic representation of basic cobalt carbonate structure [24]

On the other side, elimination of water molecules can occur with the interaction between adjacent hydroxyl groups by transfer of proton, $2OH^- \rightarrow O^{2-}+H_2O$ (ads). In principle, there is an increase in the activation energy observed at the end of dehydroxylation step due to the distance between the residual $OH^-$ groups [25]. Accordingly, the activation energy of dehydroxylation in the range of $0.05<\alpha<0.85$, is relatively constant as a result of water evolution from precursor through interlayer channels without significant diffusion. While the activation energy of the second step reaction (Fig. 6(b)) is relatively constant at the first stage of reaction and then gradually increases. It can be concluded that the second processes, i.e., dioxide carbon removing and $Co_3O_4$ nucleation and growth are, in turn, a complex solid-state reaction. Low activation energy at the beginning of the second process can be attributed to the synergetic force of $H_2O$ vapor from the first step during $CO_2$ evolution. Moreover, by increasing of $\alpha$ ($\alpha\geq0.3$), $E_a$ was increased dramatically due to the inhibition of $CO_2$ removing from the interior particle reaction interfaces by product layers.

The experimental $f(\alpha)$ curve (Fig. 8) calculated from the Arshad−Maaroufi method (Eqs. (7) and (8)) shows that the dehydration of n-BCoC depicts a fair agreement with the 2nd order exponential growth (or decay) function given as

$$f(\alpha)=f_0(\alpha)+f_1(\alpha)+f_2(\alpha)=f_0(\alpha)+A_1\exp(\alpha/k_1)+A_2\exp(\alpha/k_2) \quad (10)$$

where $f_0(\alpha)$ is constant called offset; $A_1$ and $A_2$ are also the constants known as amplitudes which probably are the frequency factors of two competitive growth reactions; and $k_1$ and $k_2$ are the growth constants of those reactions. The relative comparison of growth constants describes that the 2nd reaction is almost five times faster than the first one.

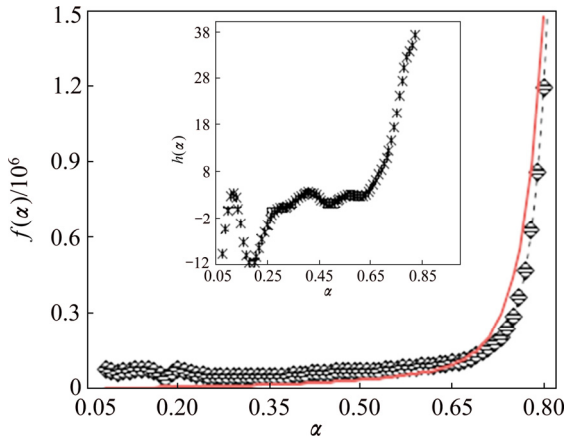


**Fig. 8** Experimental dehydration $f(\alpha)$ curve at $\beta$=5 °C/min (diamond) and theoretical fit by 2nd order exponential growth function (red line) ($k_1$=0.035 $min^{-1}$, $k_2$=0.18 $min^{-1}$. Inside is experimental dehydration $h(\alpha)$ curve)

Based on deconvoluted peaks of the first and second process data, the $h(\alpha)$ curves for each decomposition step at 5 °C/min according to the Arshad–Maarroufi method (Eq. (7)) are plotted in Fig. 9. By using the truncated Šesták–Berggren model ($f(\alpha)=c\alpha^m(1-\alpha)^n$) [26], that exactly matches any kinetic model functions and by fitting $c$, $m$ and $n$ parameters, equation equivalent to the experimental $f(\alpha)$ (Table 2) obtained by Eq. (8). As seen from Fig. 9, the trend of the first and second $h(\alpha)$ curves of thermal decomposition process follows $F_n$ and $A_n$ type model functions, respectively. It can be observed that the reaction mechanism of the process can be kinetically characterized by a reaction order step followed by the Johnson−Melh−Avrami reaction type ($A_n$). Accordingly, the kinetic model functions obtained by Eq. (8) for the first step decomposition of n-BCoC match the chemical reaction in the interphase and phase boundary development to the inside of the particles, i.e., ($F_{2/3}$) and the second decomposition step obeys $A_{3/2}$ nucleation and growth kinetic model.

Figure 10 shows that the typically normalized $f(\alpha)/f(0.5)$ plot of overall reaction ($\beta$=5 °C/min) with theoretical $f(\alpha)/f(0.5)$ plots corresponds to some of the common kinetic models. As shown, the overall complex reaction obeys the chemical reaction order ($F_n$) model to be about $\alpha$=0.45 and after that Johnson−Melh−Avrami

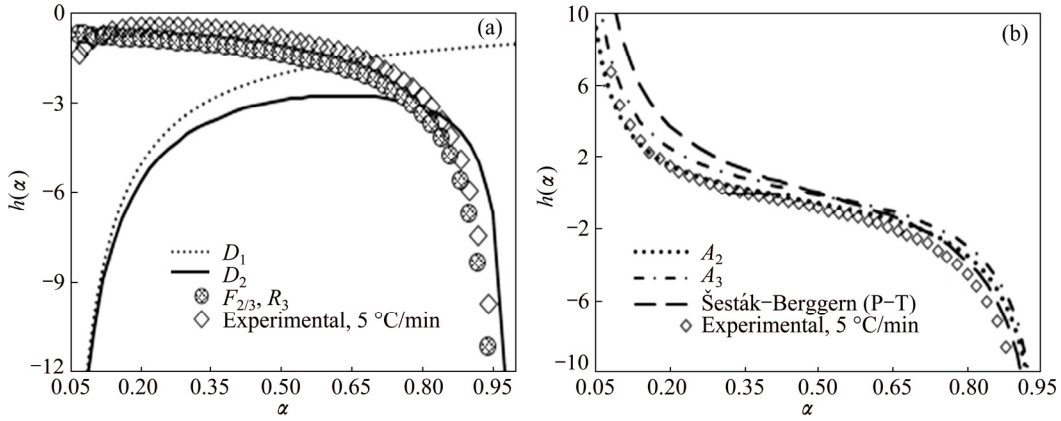


**Fig. 9** $h(\alpha)$ curves of common decelerating and nucleation and growth kinetic models with dehydroxylation (a) and decarbonation (b) steps of n-BCoC decomposition at 5 °C/min ($A_n$—Avrami-Erofeev $n$th order random nucleation and growth; $D_n$—$n$th dimensional diffusion; $F_{2/3}$ ($R_3$)—Contracting sphere reaction model; P−T: Prout−Tompkins model

**Table 2** Algebraic expressions for $f(\alpha)$ functions of anhydride n-BCoC decomposition and their corresponding equivalent reduced Šesták–Berggren equations

| Step | Mechanism | Symbol | $f(\alpha)$ | Equivalent reduced Šesták−Berggren equation |
|---|---|---|---|---|
| I | Chemical reaction order (Phase boundary controlled reaction) | $F_{2/3}(R_3)$ | $3(1-\alpha)^{2/3}$ | $3(1-\alpha)^{2/3}$ $c$=3, $m$=0, $n$=2/3 |
| II | Random instant nucleation and growth of nuclei (Avrami−Erofeev equation) | $A_{3/2}$ | $1.5(1-\alpha)(-\ln(1-\alpha))^{1/3}$ | $1.53\alpha^{0.341}(1-\alpha)^{0.867}$ $c$=1.5, $m$=0.341, $n$=0.867 |

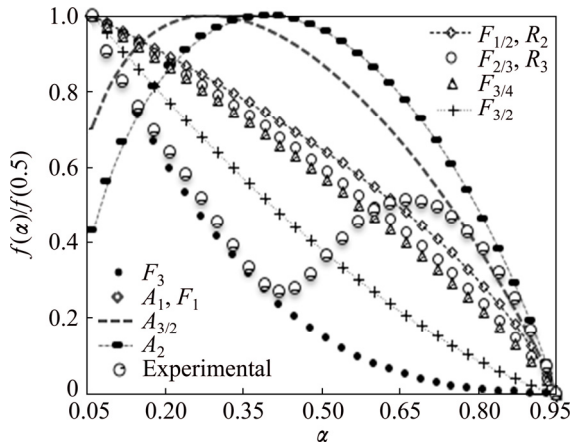


**Fig. 10** Comparison of experimental $f(\alpha)/f(0.5)$ plot of overall reaction with theoretical normalized $f(\alpha)/f(0.5)$ plots corresponding to some of most common kinetic models

type function. Since the mean activation energy is used for evaluating of $f(\alpha)/f(0.5)$ plots, the model mechanism obtained with this method is not consistent accurately with the Arshad−Maaroufi kinetic modeling method. However, the overall trend of reactions is the same in both methods. The overall reaction rate of complex reaction (consecutive) can be expressed as a function of individual reactions rate:

$$\left(\mathrm{d}\alpha/\mathrm{d}t\right)_\alpha = \sum_{i=1}^{m} l_i \left(\frac{\mathrm{d}\alpha_i}{\mathrm{d}t}\right)_\alpha = \sum_{i=1}^{m} l_i A_{i,\alpha} \exp\left(-\frac{E_i}{RT}\right) f_i(\alpha) \quad (11)$$

where $A_i$, $E_i$, $l_i$ and $f_i(\alpha)$ are the pre-exponential factor, activation energy, statistical mass and model of each unit reaction existing in overall reaction, respectively. Accordingly, truncated Šesták–Berggren model $f(\alpha)=c\alpha^m(1-\alpha)^n$ can be written as the combination of the common kinetic model functions with the master plots criteria. Hence, according to Fig. 10 and $c$, $m$ and $n$ values (Table 2), the following kinetic model functions for overall complex decomposition of anhydride n-BCoC can be obtained:

$$F(\alpha) = \begin{cases} F_n, & 0.05 < \alpha \le 0.45 \\ A_n, & 0.45 \le \alpha < 0.95 \end{cases} \quad (12)$$

By virtue of the above obtained kinetic models (Table 2), the pre-exponential coefficient can be expressed as a function of the reacted fraction of each reaction step ($\alpha$) using activation energy function, $E=F(\alpha)$ found by the isoconversional method and basic kinetic equation (Eq. (2)). The mean values of the pre-exponential coefficient for the first and second steps of anhydride n-BCoC decomposition reaction were $1.2\times10^{13}$ and $3.2\times10^{17}$ $s^{-1}$, respectively.

### 4.3 Morphological changes in sample and reaction mechanism

The morphologies of precursor and its calcination product at 300 °C are shown in Fig. 11. The precursor (Fig. 11(a)) has the appearance of aggregates of

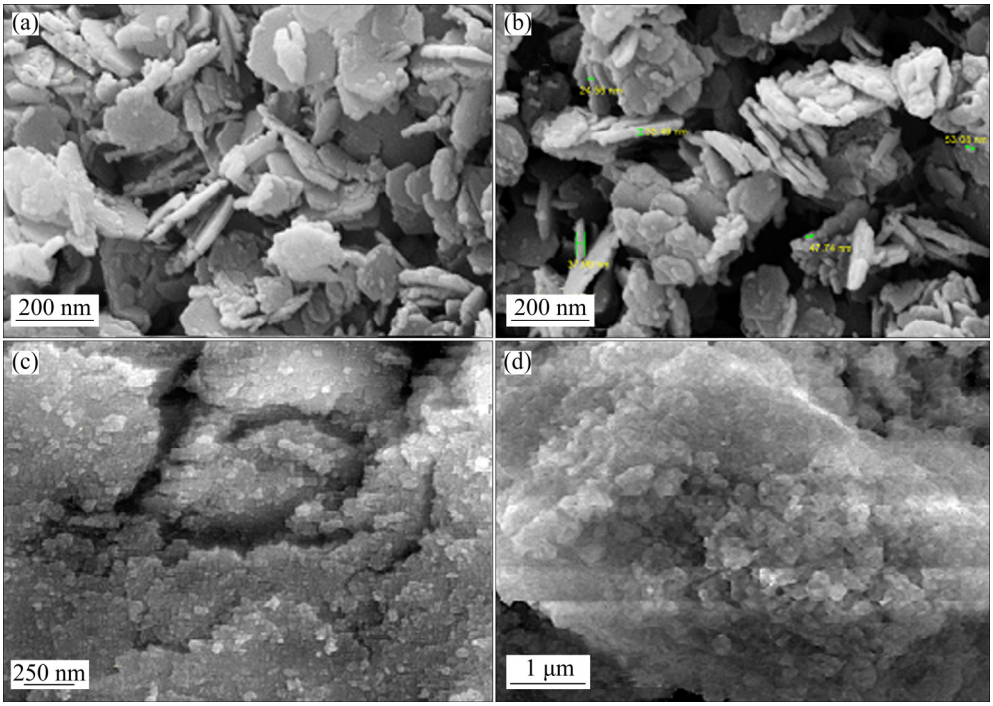


**Fig. 11** FESEM images of precursor (a) and its calcination product (b, c and d) at 300 °C for 2 h in air

nanometric plates, where the coherence of the platelets is obvious. As shown from Figs. 11(c) and (d), at the end of reaction, the platelets are gradually sintered and form a relatively smooth surface, hence impedes the diffusional removal of $CO_2$ generated by the second step reaction. This inhibition of $CO_2$ may be the possible cause of tail at the end of the second reaction step in TG curves (Fig. 2). The evolved $CO_2$ gas escapes through the cracks formed on the surface of product layer (Fig. 11(c)). In addition, according to XRD results of the precursor at 300 °C, nucleation and growth of product phase, $Co_3O_4$, on the surface of platelets can be seen at this temperature (Fig. 11(d)). The products have generally nanosheet morphology and relatively narrow size distribution. This morphology is similar to the crystal of $Co_3O_4$ that is obtained from cobalt hydroxide carbonates synthesized by hydrothermal methods [27]. The planar morphology obtained by thermal decomposition of n-BCoC favors the formation of well-crystallized nanosheets of $Co_3O_4$ and thermal decomposition conditions necessary for a collective topotactic transformation are preserved.

In summary, the consecutive thermal decomposition of anhydride n-BCoC involves the following processes:

1) The onset of hydroxide component decomposition ($Co(OH)_2$), in progressing of simultaneous dehydroxylation and the beginning of carbonate phase decarbonation ($\alpha_1$=0.65);

2) Completion of dehydroxylation step ($\alpha_2$=0.25), and after a while;

3) Completion of decarbonation with tailed gas evolution ($CO_2$ from internal particles or $O_2$ from the non-stoichiometric product ($Co_3O_{4+x}$) [22]).

Therefore, two steps of decomposition (dehydroxylation and decarbonation) are performed in the common range of temperature and hence can influence the mechanism of each other. Water vapor from the first step can facilitate removing of $CO_2$ resulted from carbonate component decomposition at the beginning of the second step decomposition. On the other side, gases product of the second step helps to drive away residual water at the next remaining half of reaction.

## 5 Conclusions

Complex thermal decomposition of n-BCoC synthesized from spent lithium-ion batteries accompanied by overlapping reaction traces, due to the occurrence of various physico−chemical processes. Fraser–Suzuki fitting function was used to deconvolute the overlapping complex thermal decomposition of n-BCoC. Advanced kinetic modeling (Arshad−Maaroufi) and combined modeling method were used to study the individual reaction kinetics, separately. The thermal decomposition of anhydride n-BCoC concludes two simultaneous reactions, i.e., dehydroxylation and carbonate phase decomposition. The dehydroxylation precedes carbonate decomposition and each step is influenced by the other. Thermogravimetry analysis of n-BCoC showed that decomposition temperatures shifted to lower ones compared with the microparticle size

reactant. It is found that the structure of reactant is one of the important factors which identifies the mechanism of decomposition and the reaction pathway of nano-structures is different from that of the bulk material.

## Acknowledgments

This work was supported by the Iranian National Science Foundation (INSF).

## References

[1] JOULIÉ M, LAUCOURNET R, BILLY E. Hydrometallurgical process for the recovery of high value metals from spent lithium nickel cobalt aluminum oxide based lithium-ion batteries [J]. Journal of Power Sources, 2014, 247: 551−555.

[2] BARIK S P, PRABAHARAN G, KUMAR B, An innovative approach to recover the metal values from spent lithium-ion batteries [J]. Waste Management, 2016, 51: 222−226.

[3] ANDO M, KOBAYASHI T, IIJIMA S, HARUTA M. Optical recognition of CO and $H_2$ by use of gas-sensitive Au−$Co_3O_4$ composite films [J]. J Mater Chem, 1997, 7(9) : 1779−1783.

[4] ZHANG Z, GENG H, ZHENG L, DU B. Characterization and catalytic activity for the NO decomposition and reduction by CO of nanosized $Co_3O_4$ [J]. Journal of Alloys and Compounds, 2005, 392(1−2): 317−321.

[5] YANG J J, CHENG H, FROST R L. Synthesis and characterisation of cobalt hydroxy carbonate $Co_2CO_3(OH)_2$ nanomaterials [J]. Spectrochimica Acta, Part A: Molecular and Biomolecular Spectroscopy, 2011, 78(1): 420−428.

[6] WANG S L, QIAN L Q, XU H, LU G L, DONG W J, TANG W H. Synthesis and structural characterization of cobalt hydroxide carbonate nanorods and nanosheets [J]. Journal of Alloys and Compounds, 2009, 476(1−2): 739−743.

[7] XING W, ZHUO S, CUI H, ZHOU H, SI W, YUAN X, GAO X, YAN Z. Morphological control in synthesis of cobalt basic carbonate nanorods assembly [J]. Materials Letters, 2008, 62(8−9): 1396−1399.

[8] AKBARI GARAKANI M, ABOUALI S, ZHANG B, TAKAGI C A, XU Z L, HUANG J Q, HUANG J, KIM J K. Cobalt carbonate/and cobalt oxide/graphene aerogel composite anodes for high performance Li-ion batteries [J]. ACS Applied Materials and Interfaces, 2014, 6(21): 18971−18980.

[9] EL-SHOBAKY G A, AHMAD A S, AL-NOAIMI A N, EL-SHOBAKY H G. Thermal decomposition of basic cobalt and copper carbonates: Thermal stability of the produced oxides as influenced by gamma-irradiation [J]. J Therm Anal Calorim, 1996, 46(6): 1801−1808.

[10] MEHANDJIEV D, NIKOLOVA-ZHECHEVA E. Mechanism of the decomposition of cobaltous compounds in vacuo [J]. Thermochimica Acta, 1980, 37(2): 145−154.

[11] ROMERO M M, LLOPIZ J C, JEREZ A, PICO C, VEIGA M L. Kinetic study by mass spectrometry of the decomposition of basic cobalt carbonate [J]. Thermochimica Acta, 1990, 168: 53−57.

[12] PEREJON A, SANCHEZ-JIMENEZ P E, CRIADO J M, PEREZ-MAQUEDA L A. Kinetic analysis of complex solid-state reactions: A new deconvolution procedure [J]. Journal of Physical Chemistry B, 2011, 115(8): 1780−1791.

[13] DORELLA G, MANSUR M B. A study of the separation of cobalt from spent Li-ion battery residues [J]. Journal of Power Sources, 2007, 170(1): 210−215.

[14] WANG R C, LIN Y C, WU S H. A novel recovery process of metal values from the cathode active materials of the lithium-ion secondary batteries [J]. Hydrometallurgy, 2009, 99(3−4): 194−201.

[15] LI L, GE J, CHEN R, WU F, CHEN S, ZHANG X. Environmental friendly leaching reagent for cobalt and lithium recovery from spent lithium-ion batteries [J]. Waste Management, 2010, 30(12): 2615−2621.

[16] FRASER R D B, SUZUKI E. Resolution of overapping bands: Functions for simulating band shapes [J]. Analytical Chemistry, 1969, 41(1): 37−39.

[17] VYAZOVKIN S. Kinetic concepts of thermally stimulated reactions in solids: A view from a historical perspective [J]. International Reviews in Physical Chemistry, 2000, 19: 45−60.

[18] ARSHAD M A, MAAROUFI A K. An innovative reaction model determination methodology in solid state kinetics based on variable activation energy [J]. Thermochimica Acta, 2014, 585: 25−35.

[19] SHAHCHERAGHI S H, KHAYATI G R, RANJBAR M. An advanced reaction model determination methodology in solid-state kinetics based on Arrhenius parameters variation, Part I: Thermal dehydration kinetic analysis of $Cu_4SO_4(OH)_6$ [J]. Journal of Thermal Analysis and Calorimetry, 2015, 122: 175−188.

[20] XU R, ZENG H C. Dimensional control of cobalt-hydroxide-carbonate nanorods and their thermal conversion to one-dimensional arrays of $Co_3O_4$ nanoparticles [J]. Journal of Physical Chemistry B, 2003, 107(46): 12643−12649.

[21] HOSHYAR R, KHAYATI G R, POORGHOLAMI M, KAYKHAII M. A novel green one-step synthesis of gold nanoparticles using crocin and their anti-cancer activities [J]. Journal of Photochemistry and Photobiology B: Biology, 2016, 159: 237−242.

[22] ARDIZZONE S, SPINOLO G, TRASATTI S. The point of zero charge of $Co_3O_4$ prepared by thermal decomposition of basic cobalt carbonate [J]. Elecrrochimica Acta, 1995, 40(16): 2683−2686.

[23] MANSOUR S A A. Spectrothermal studies on the decomposition course of cobalt oxysalts, Part I: Basic cobalt carbonate [J]. Materials Chemistry and Physics, 1994, 36: 309−316.

[24] RAMESH T N. Polytypic transformations during the thermal decomposition of cobalt hydroxide and cobalt hydroxynitrate [J]. Journal of Solid State Chemistry, 2010, 183(6): 1433−1436.

[25] NITYASHREE N, GAUTAM U K, RAJAMATHI M. Synthesis and thermal decomposition of metal hydroxide intercalated saponite [J]. Applied Clay Science, 2014, 87: 163−169.

[26] PÉREZ-MAQUEDA L A, CRIADO J M, SÁNCHEZ-JIMÉNEZ P E. Combined kinetic analysis of solid-state reactions: A powerful tool for the simultaneous determination of kinetic parameters and the kinetic model without previous assumptions on the reaction mechanism [J]. Journal of Physical Chemistry A, 2006, 110(45): 12456−12462.

[27] WANG J, NIU B, DU G, ZENG R, CHEN Z, GUO Z, DOU S. Microwave homogeneous synthesis of porous nanowire $Co_3O_4$ arrays with high capacity and rate capability for lithium ion batteries [J]. Materials Chemistry and Physics, 2011, 126(3): 747−754.

# 由废旧锂离子电池合成碱式碳酸钴纳米片的热分解动力学：重叠复杂反应的反卷积

Hossein EBRAHIMZADE[1], Gholam Reza KHAYATI[2], Mahin SCHAFFIE[3]

1. Department of Mineral Industries Research Center,
Shahid Bahonar University of Kerman, P. O. Box No. 76135-133, Kerman, Iran;
2. Department of Materials Science and Engineering,
Shahid Bahonar University of Kerman, P. O. Box No. 76135-133, Kerman, Iran;
3. Department of Chemical Engineering,
Shahid Bahonar University of Kerman, P. O. Box No. 76135-133, Kerman, Iran

**摘　要**：采用一种新的非等温动力学分析方法，研究由废旧锂离子电池(LIBs)合成的碱式碳酸钴纳米片(n-BCoC)的热分解动力学模拟。对线性升温速率条件下获得的总微分热重曲线，运用 Fraser−Suzuki 函数进行重叠复杂过程的反卷积，然后用一种新的动力学分析方法对各个离散过程进行动力学分析。结果表明，在 136~270 °C 范围内，n-BCoC 在空气中的分解是通过两个连续反应进行的。n-BCoC 的分解过程是从氢氧化物 $Co(OH)_2$ 的分解开始的，直到(失重)65%；同时碳酸盐相也开始脱碳。脱碳过程持续进行，释放出 $CO_2$，最终形成碳酸钴纳米片。整个过程的反应机理可用两个连续反应描述：一个是相边界收缩反应，另一个符合 Avrami−Erofeev 方程。动力学研究得到的(反应)机制信息与傅里叶变换红外光谱和扫描电镜的分析结果吻合较好。

**关键词**：动力学模拟；碱式碳酸钴纳米片(n-BCoC)；重叠反应；废旧锂离子电池

**(Edited by Xiang-qun LI)**